Improved Short-Term Frequency Stability of a Rubidium Atomic Fountain Clock Using a Cryogenic Sapphire Oscillator

Dan-Dan Liu(刘丹丹)[1,2], Si-Chen Fan(范思晨)[1,2],Wen-Yu Zhao(赵文宇)[1,2], Yong Guan(管勇)[1,2], Hui Zhang(张辉)[1,2], Xin-Liang Wang(王心亮)[1,2], Yang Bai(白杨)[1,2], Shao-Shao Yu(鱼少少)[1,2] , Jun Ruan(阮军)[1,2,†] and Shou-Gang Zhang(张首刚) [1,2]

[1]*National Time Service Center, Chinese Academy of Sciences, Xi’an 710600, China*
[2]*Key Laboratory of Time Reference and Applications, Chinese Academy of Sciences, Xi’an 710600, China*

This work demonstrates the integration of a cryogenic sapphire oscillator (CSO) into a rubidium atomic fountain clock. After stabilization of its frequency and output power, the free-running CSO output is compared with that of a reference hydrogen maser and phase-locked to it with a 400 s servo time constant. The 100 MHz CSO signal locked to the hydrogen maser is transmitted to the laboratory housing the rubidium fountain clock via fiber-optic microwave frequency transfer. A frequency synthesizer uses this reference signal to generate the 6.834 GHz Ramsey interrogation signal, replacing the original local oscillator in the fountain clock. As a result, the frequency stability is improved from $2.7\times10^{-13}\tau^{-1/2}$ to $9.0\times10^{-14}\tau^{-1/2}$. The dominant noise sources currently limiting further improvement are also identified and analyzed. Background atoms are found to be the primary limitation under the present experimental conditions.

Keywords: atomic fountain clock, frequency instability, cryogenic sapphire oscillator, fiber-optic microwave frequency transfer

PACS: 06.30.Ft, 07.05.Fb, 07.77.Gx

1. Introduction

Atomic fountain clocks exhibit the lowest frequency instability among microwave clocks and play a crucial role in global timekeeping systems, searches for temporal variations of fundamental constants, and measurement of the rubidium ground-state hyperfine transition frequency.[1-3] Rubidium atomic fountain clocks, characterized by excellent frequency stability and ultra-low frequency drift, are assigned the maximum weight in the generation of International Atomic Time (TAI).[4] The frequency stability of a fountain clock is limited by several noise sources: quantum projection noise (QPN) arising from the finite number of detected atoms, technical noise sources such as microwave phase noise, detection laser frequency noise, and electronic noise.[5] In a pulsed fountain clock, atoms are prepared, launched, interrogated, and detected periodically. The microwave interrogation signal is thus applied to the atoms only during the Ramsey interrogation period, while the remaining time is occupied by dead times such as atomic cooling and launching. The Dick effect describes the process in which this unsampled low-frequency phase noise of the local oscillator (LO) is down-converted into the clock's operating bandwidth, thereby degrading the clock's frequency stability.

To overcome this limitation, two types of local oscillators have been developed: optical microwave sources and cryogenic sapphire oscillators (CSOs). They exhibit

† Corresponding author. E-mail:ruanjun@ntsc.ac.cn

excellent short-term frequency stability at the 10^{-15} level.[6-11] Many research institutions have integrated optical microwave sources or CSOs into cesium fountain clocks, reducing the frequency instability to the order of 10^{-14}.[12-19] At Observatoire de Paris (OP) and National Metrology Institute of Japan (NMIJ), CSO have been introduced into their cesium fountain clocks. The three French fountain clocks have demonstrated 1 s fractional frequency instabilities ranging from 1.6×10^{-14} to 7.0×10^{-14},[12–13] while NMIJ-F2 has achieved a 1 s instability in the range of 8.3×10^{-14} to 2×10^{-13}.[14–15] Physikalisch-Technische Bundesanstalt (PTB) has used optically generated microwave sources as local oscillators in two cesium fountain clocks, improving their 1 s instabilities to 7.2×10^{-14} and 2.5×10^{-14} respectively.[16-17] In China, National Time Service Center (NTSC) and National Institute of Metrology (NIM) have also demonstrated the use of optically generated microwave sources in cesium fountain clocks,[18-19] although such systems have not yet been employed for long-term routine operation in fountain clocks. These representative examples show that improving the local oscillator plays an important role for enhancing the performance of atomic fountain clocks.

The CSO provides a signal with sufficiently low phase noise to mitigate the Dick effect while maintaining drift rates orders of magnitude lower than those of optical-microwave sources. These attributes make the CSO a preferred oscillator for practical fountain clocks, particularly for autonomous long-term operation.

At the NTSC, two rubidium fountain clocks (NTSC-RbF1 and NTSC-RbF2) are operational. NTSC-RbF1 operates continuously to contribute to TAI. To avoid interrupting its regular contribution, experiments are performed on NTSC-RbF2.

Section 2 provides a theoretical analysis of the factors affecting the short-term frequency instability of atomic fountain clocks. Section 3 describes the details of the experimental measurement procedures and results, and Section 4 analyzes and discusses the factors limiting further improvement in frequency instability based on the experimental results, and Section 5 summarizes the conclusions.

2. Theoretical analysis of the frequency stability

The Allan deviation of the frequency stability of the atomic fountain clocks can be modeled as:[5]

$$\sigma_y(\tau) = \frac{1}{\pi Q_{at}}\sqrt{\frac{T_c}{\tau}}\left(\frac{1}{N_{at}} + \frac{1}{N_{at}n_{ph}} + \frac{2\sigma_{\delta N}^2}{N_{at}^2} + \gamma\right)^{1/2} \quad (1)$$

where τ is the integration time in seconds, Tc is the fountain cycle. N_{at} represents the total number of atoms, which is related to quantum projection noise. In each fountain cycle, N_{at} is determined by adding together the number of detected atoms in the two hyperfine levels. n_{ph} represents the photon shot-noise of the detection fluorescence. $\sigma_{\delta N}^2$ is the variance of the atom number fluctuations. γ represents the LO noise. When the number of photons emitted by each atom is greater than 150 and the fluorescence collection efficiency is favorable (>10%), the contributions by the second and third terms on the right-hand side of equation (1) can be neglected. The frequency stability of the fountain clock is mainly limited by the number of detected atoms and the phase noise of the LO.

Eq. (1) represents the complete model for the Allan deviation, whereas Eq. (2) relates the Allan deviation to the transition-probability fluctuation.[20] It is applicable when the LO noise is negligible and the Ramsey fringe is locked at half-maximum, so that P≃ 1/2. Under these conditions, $\sigma_p/P=1/SNR=1/N_{at}$, where the *SNR* is limited by quantum projection noise. If the LO noise is not negligible, the full expression in Eq. (1) should be used, with the LO contribution represented by γ. The simplified form therefore applies only under the above conditions:

$$\sigma_y(\tau) = \frac{1}{\pi Q_{at}} \frac{1}{\sqrt{N_{at}}} \sqrt{\frac{T_c}{\tau}} \tag{2}$$

3. Experiments

The experimental setup consists of three parts, as shown in Fig. 1. The first part presents the operating principle of the CSO. Its free-running 10 GHz output is divided down to 100 MHz and phase-locked to a hydrogen maser. The second part describes the transmission of the stabilized 100 MHz CSO signal over a 100 m spooled fiber. The third part demonstrates the operation of the rubidium fountain clock using the CSO as the LO. A 6.834 GHz microwave signal is generated via a frequency synthesizer from the 100 MHz signal of the CSO and is supplied to the Ramsey cavity. The frequency offset between the atomic resonance frequency and the microwave frequency is calculated, and the resulting error signal is fed back to the direct digital synthesizer (DDS) to lock the microwave frequency to the atomic transition.

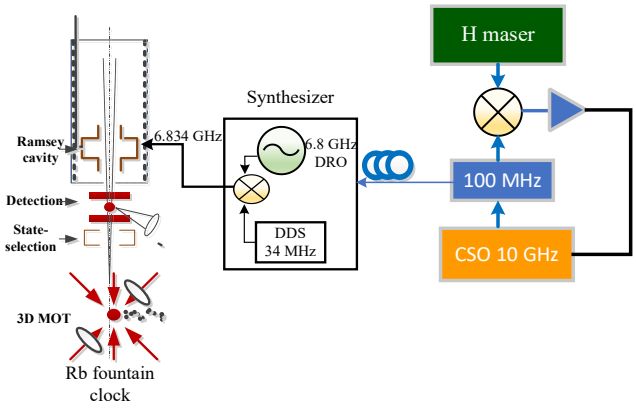


Fig. 1. Experimental setup of the rubidium fountain clock with CSO and fiber transfer

3.1. CSO

The CSO uses a sapphire resonator as its core component. It operates in the whispering-gallery mode (WGM). In this mode, electromagnetic waves undergo continuous total internal reflection at the inner surface of the cylindrical surface and propagate along the medium. Consequently, the electromagnetic energy is confined to a small annular region near the dielectric surface. At liquid-helium temperature, the resonator achieves a quality factor (Q) exceeding 1×10^8. The CSO employed in this work is equipped with a pulse-tube cryocooler developed by the FEMTO-ST Institute. The pulse-tube cryocooler transfers heat through solid thermal links, requiring no refill of cryogenic liquids and enabling continuous, maintenance-free operation. The phase noise of the 100 MHz CSO output is characterized by comparison with 5 MHz signal of an ultra-stable oscillator HSO-14. As shown in Fig. 2, the phase noise of the CSO is -135 dBc/Hz at a 1 Hz offset. The glitches in Fig. 2 are caused by the 50 Hz

AC power supply frequency and its harmonics. The phase noise at 6.8 GHz is theoretically estimated to be -98 dBc/Hz at a 1 Hz offset. The free-running CSO exhibits frequency drift. A monitoring system measures the phase difference between a hydrogen maser and the CSO. An error signal is fed back to the DDS inside the CSO. This phase lock is based on a 100 MHz beatnote. The CSO is phase locked to the hydrogen maser with a bandwidth of 0.4 mHz and a servo time constant of 400 s.

Frequency stability measurements are performed using a phase noise analyzer VCH-323. After the CSO is phase-locked to the hydrogen maser, it is then compared against this hydrogen maser. Figure 3 shows the Allan deviation of the CSO in free-running mode (black squares) and in phase-locked mode (red circles) , measured by comparison against the hydrogen maser. For 1 s ≤ τ ≤ 100 s, the two Allan deviation curves essentially overlap. For time longer than 100 seconds, the black square curve deviates from $\tau^{-1/2}$ slope because of the drift of the CSO, whereas the curve for the phase-locked CSO continues to decrease as the integration time increases. By locking the CSO to the hydrogen maser, we can integrate the short-term frequency stability of the CSO and the long-term stability of the hydrogen maser.

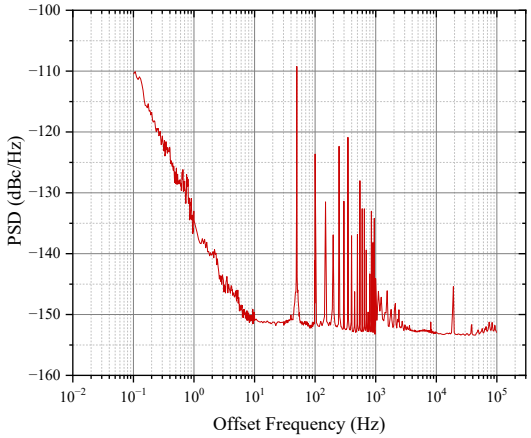


Fig. 2. 100 MHz phase noise of the CSO

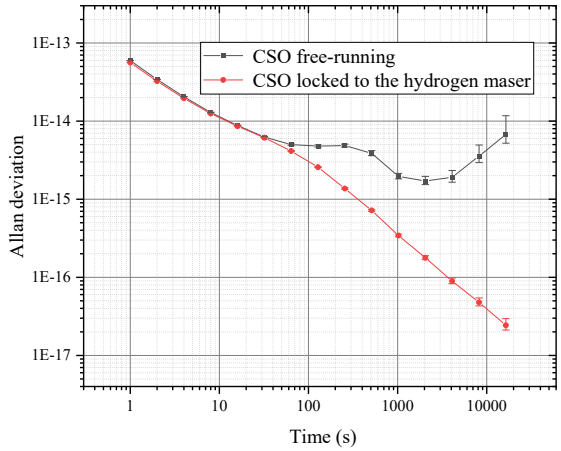


Fig. 3 . Frequency stability of the CSO in free-running and locked status

3.2. Transferring the CSO signal

The CSO and the rubidium fountain clock NTSC-RbF2 are located in two laboratories separated by approximately 100 m. To transfer the ultra-stable CSO frequency reference to the fountain clock, we employ a fiber-optic microwave

frequency-transfer system developed at NTSC.

The architecture of the transmission system is schematically shown in Fig. 4.[21] At the transmitter, the 100 MHz CSO output is multiplied up to 3.6 GHz. One of the 3.6 GHz signal is mixed with the 9 GHz signal generated by the voltage-controlled oscillator (VCO), and the other is mixed with the signal detected locally after round-trip propagation over the fiber link. These two mixed outputs are further mixed to generate an error signal for tuning the VCO frequency. At the receiver, the received 9 GHz signal is split into two branches. One branch is divided by four to generate 2.25 GHz for return transmission, while the other is divided by multi-stage frequency dividers to produce the 100 MHz reference output. This closed-loop feedback system based on phase-locked loop (PLL) technology compensates for fiber-induced phase noise and ensures that the phase of the microwave signal at the receiver is locked to the reference signal at the transmitter, thereby achieving high-precision phase-stable transmission. In order to evaluate the degradation introduced by the fiber link, the CSO signal transmitted through a 100 m spooled optical fiber and the local CSO signal are compared using the VCH-323. As shown in Fig. 5, a frequency-transfer instability of 1.4×10^{-14} at 1 s integration time is obtained. This residual transfer instability may be attributed to mechanical vibration from the CSO cryocooler compressor coupling to the spooled fiber. Further investigation and vibration isolation improvements will be carried out.

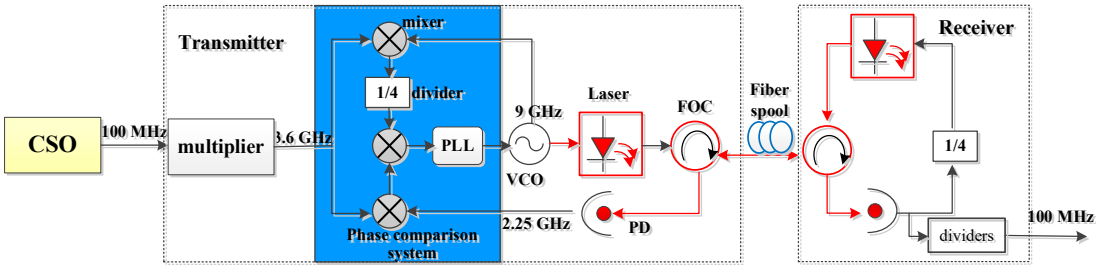


Fig. 4 . Architecture of the fiber-based microwave frequency- transfer FOC: Fiber optic circulator; PD: Photoelectric detector

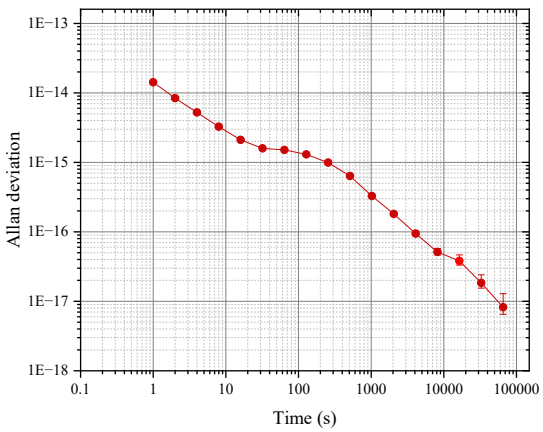


Fig. 5 . Frequency stability of the transmitted CSO signal against the original CSO signal

3.3. Frequency instability measurements using the CSO

The 100 MHz CSO signal locked to the hydrogen maser is transmitted to the rubidium fountain clock laboratory via the deployed optical fiber. The rubidium atoms

are trapped directly from the background vapor into a three-dimensional magneto-optical trap (MOT) configuration without a 2D MOT. The detailed physical structure of the rubidium fountain clock have been reported elsewhere [22] and is not repeated here.

To generate the microwave frequency required for the Ramsey cavity, a 6.8 GHz signal from a dielectric resonator oscillator (DRO) and a 34 MHz signal from a DDS are mixed using a combination of DDS and PLL technologies. The transmitted 100 MHz CSO signal is split by a power divider and used as the common frequency reference for both the DRO and the DDS. The 6.8 GHz synthesizer is described in detail in Ref. [23]. The residual phase noise of the frequency synthesizer is reported as -85 dBc/Hz at a 1 Hz offset. The transmitted 100 MHz CSO signal is compared with HSO-14, the resulting phase noise is measured to be -110 dBc/Hz at 1 Hz offset, as shown in Fig. 6. A theoretical estimation at 6.8 GHz yields an absolute phase noise of approximately -73 dBc/Hz. By fitting the phase noise data over the offset frequency range from 1 Hz to 20 Hz, the resulting Dick-effect contribution to the short-term frequency stability of the rubidium fountain clock is calculated to be $4.6\times10^{-14}\tau^{-1/2}$.

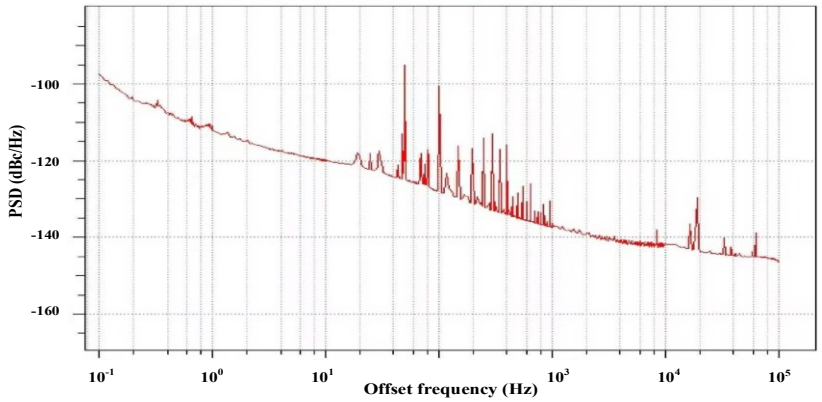


Fig. 6. Phase noise of the transmitted 100 MHz CSO signal

The rubidium fountain clock operates with a cycle time of 1.5 s. The microwave frequency is locked to the atomic resonance by alternating the frequency between $f_0\pm\nu/2$. f_0 is the central Ramsey resonance frequency, ν is the full width at half maximum of the Ramsey fringes. A feedback correction is applied to the 34 MHz DDS every two fountain cycles. A self-developed frequency-locking program is implemented. The frequency instability of the rubidium fountain clock is characterized against the hydrogen maser and the CSO. As shown in Fig. 7, the frequency instability of NTSC-RbF2 is reduced from $2.7\times10^{-13}\tau^{-1/2}$ to $9.0\times10^{-14}\tau^{-1/2}$ after integrating the CSO as the local oscillator, corresponding to a nearly threefold improvement in performance.

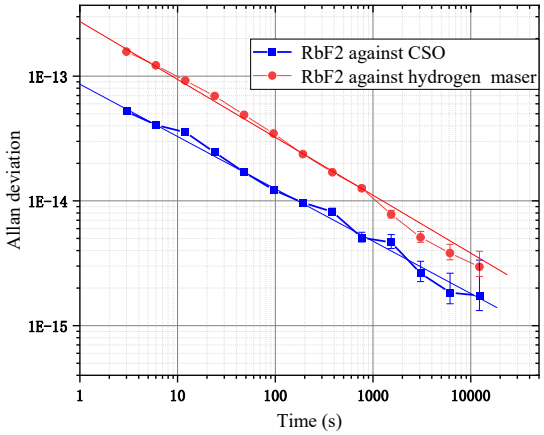


Fig. 7. Measured Allan deviations of the frequency of NTSC-RbF2 using the CSO and hydrogen maser

4. Discussion

To obtain a theoretical estimate of the frequency stability, the number of atoms N_{at} is varied by adjusting the microwave power in the state-selection cavity. When the interrogation microwave power is set at the $\pi/2$ transition and the interrogation frequency is offset by 0.5 Hz from the central atomic resonance frequency. For each atom number N_{at}, the atomic transition probability P is measured 500 times, the variance of the transition probability fluctuation σ_P is calculated.

Combining Eqs. (1) and (2), σ_P^2 can be expressed as (3):

$$\sigma_P^2 = P^2\left(\frac{1}{N_{at}} + \frac{1}{N_{at}n_{ph}} + \frac{2\sigma_{\delta N}^2}{N_{at}^2} + \gamma\right) \tag{3}$$

where P is 1/2. Therefore, the fitting function is chosen as:

$$y=0.25*(a/x+b/x^2+c) \tag{4}$$

where y denotes σ_P^2 and x denotes the relative atom number. The fitting result is shown in Fig. 8. The fitted coefficient a is $2.46\times10^{-6}\pm5.26\times10^{-7}$. The fitted parameter a is used in equation (4) to estimate the effective number of atoms arriving in the detection region.

$$\frac{a}{x} = \frac{1}{N_{det}} \tag{5}$$

where a is the proportionality coefficient between the relative number of atoms and the actual number of atoms. The maximum relative atom number x is 2.65. Using this value, the detected atom number is calculated as 1.1×10^6. Frequency stability of NTSC-RbF2 under the QPN limited is expected to be $5.4\times10^{-14}\tau^{-1/2}$, which is lower than the measured value of $9.0\times10^{-14}\tau^{-1/2}$.

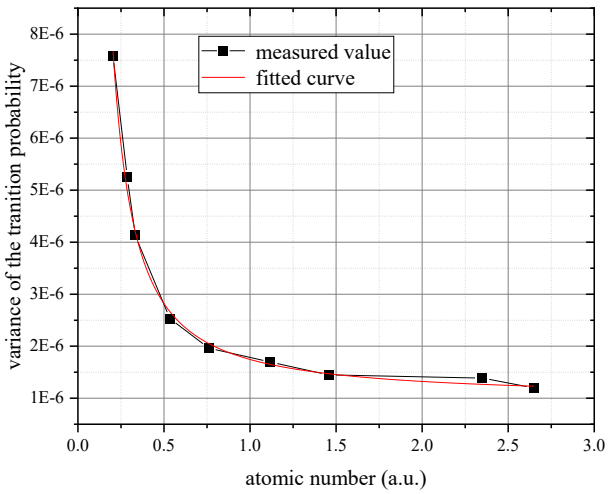


Fig. 8 . Variation with different atomic number

To investigate the discrepancy between the experimental and the theoretical values, the standard deviation of the transition probability fluctuations, denoted as σ_P is measured under several experimental conditions. The corresponding Allan deviation at 1 s is calculated using equation (2). The results are summarized in Table 1.

Under condition A, both the detection laser and the detection repumping laser are turned off, allowing measurement of the electronic noise floor of the detection system.

In condition B, only the detection repumping laser is activated. Compared with condition A, σ_P shows no significant increase, indicating that the detection repumping laser contributes negligibly to the noise.

In condition C, both the detection and detection repumping lasers are turned on, the value of σ_P increases by a factor of approximately two compared with the noise floor, reaching a level comparable to that observed during normal clock operation.

Condition D is designed to characterize the noise contribution in the absence of atomic interaction. In this case, both lasers are activated while the cooling laser frequency is detuned far from the atomic resonance. The value of σ_P under condition D is slightly higher than that under condition B.

The difference between condition C and condition D mainly reflects the presence or absence of atomic interactions.

Therefore, the increased noise observed in condition C is attributed primarily to background atoms rather than to laser or electronic noise. Because NTSC-RbF2 uses only a 3D MOT, without the background-rejection effect of a 2D MOT, the background atomic density is nearly uniform throughout the vacuum chamber, and a large number of background atoms are present near the detection region. This background-atom contribution dominates the short-term stability and is therefore the main limiting factor in the current system.

On the basis of the Rb vapor pressure at room temperature and the conductance of the fountain-clock vacuum system, the Rb background pressure is estimated to be

9×10^{-7}Pa. At approximately 300 K, this pressure corresponds to a Rb number density of about $2.2\times10^{14}/m^3$. The experimental data (Table 1) show that when the probe laser is detuned from the Rb resonance, so that the thermal background atoms contribute negligibly to the detected fluorescence, the relative probability fluctuation is 4.8×10^{-4}. When the probe laser is tuned onto the Rb resonance, the thermal background atoms are efficiently excited and generate a large, fluctuating fluorescence background, and the relative probability fluctuation increases to 8.2×10^{-4}. If these two noise contributions are independent, the background-fluorescence contribution can be isolated by subtracting the variances, yielding a background-induced standard deviation of approximately 6.65×10^{-4}. This experimentally inferred value is in excellent agreement with the estimate obtained from a background pressure of 9×10^{-7}Pa. In other words, the pressure required to reproduce the observed on-resonance/off-resonance difference is essentially the same as that used in the calculation, strongly supporting the conclusion that the additional probability fluctuation observed under resonant excitation originates from background-gas fluorescence.

Table 1. σ_P and $\sigma_y(1s)$ in different conditions

Conditions	A	B	C	D
σ_P	4.6E-4	4.8E-4	8.2E-4	5.4E-4
$\sigma_y(1s)$	5.2E-14	5.5E-14	9.4E-14	6.1E-14

5. Conclusion

By successfully transferring the CSO signal to the rubidium fountain clock using fiber-optic microwave frequency transmission technology, a nearly threefold improvement in the short-term frequency instability has been achieved, the Allan deviation is improved from $2.7\times10^{-13}\tau^{-1/2}$ to $9.0\times10^{-14}\tau^{-1/2}$. Future work will focus on further reducing the transferred frequency instability. This demonstration validates the feasibility of deploying a cryogenic sapphire oscillators in a rubidium fountain clock and paves the way for their integration into multiple atomic fountain clocks.

Data availability statement

All data that support the findings of this study are included within the article.

Acknowledgment

This work was supported by the Instrumentation Upgrade Project for the National Major Science and Technology Infrastructure: Long-and-Short-Wave Time Service System under Grant 2406-000000-04-02-594855, the Instrument Development Project of the Chinese Academy of Sciences under Grant PTYQ2025TD0014, and the National Key R&D Program of China: Rubidium Atomic Frequency Standard under

Grant 2025YFH0101204.

References

[1] Ovchinnikov Y B, Szymaniec K and Edris S 2015 *Metrologia* **52** 595

[2] Tobar M E, Stanwix P L, Abgrall M, Bize S, Clairon A, Guéna J and Laurent Ph 2012 *IEEE International Frequency Control Symposium*, May 20-24, 2012, Baltimore, Maryland, USA

[3] www.bipm.org/en/time-ftp

[4] Peil S, Akin T G and Whalen J D 2025 *Phys. Rev. A* **24** 024014

[5] Santarelli G, Laurent Ph, Lemonde P, Clairon A, Mann A G, Chang S, Luiten A N and Salomon C 1999 *Phys. Rev. Lett.* **82** 4619

[6] Hartnett J G, Nand N R and Lu C 2012 *Appl. Phys. Lett.* **100** 183501

[7] Hartnett J G, Parker S R, Ivanov E N, Povey T, Nand N R and Le Floch J M. *Electronics Letters* 2014 **50** 294

[8] Fluhr Ch, Dubois B, Guillaume Le Tetu G, Soumann V, Paris J, Rubiola E and Giordano V 2022 *arXiv* p. 1-8

[9] Fortier T M, Kirchner M S, Quinlan F, Taylor J, Bergquist J C, Rosenband T, Lemke N, Ludlow A, Jiang Y, Oates C W and Diddams S A 2011 *Nat. Photonics* **5** 425

[10] Millo J, Abgrall M, Lours M, English E M L, Jiang H, Guéna J, Clairon A, Bize S, Coq Y Le and Santarelli G 2009 *Appl. Phys. Lett.* **94** 141105.

[11] Bouchand R, Xie X P, Giunta M, Haensel W, Lezius M, Holzwarth R, Alexandre Ch, Tremblin P A, Santarelli G and Coq Y Le 2017 *Photon. Technol. Lett.* **29** 1403.

[12] Guéna J, Abgrall M, Rovera D, Rosenbusch P, Chupin B, Lours M, Santarelli G, Laurent P, Bize S, Clairon A and Tobar M 2011 *Joint Conference of the IEEE International Frequency Control Symposium/European Frequency And Time Forum Proceedings* p. 615

[13] Abgrall M, Guéna J, Lours M, Santarelli G, Tobar M E, Bize S, Grop S, Dubois B, Fluhr Ch and Giordano V 2016 *IEEE Transactions on Ultrasonics, Ferroelectrics, and Frequency Control* **63** 1198

[14] Takamizawa A, Yanagimachi S, Tanabe T, Hagimoto K, Hirano I, Watabe K, Takeshi I and Hartnett J G 2014 *IEEE Transactions on Ultrasonics, Ferroelectrics, and Frequency Control* **61** 1463

[15] Takamizawa A, Yanagimachi S and Hagimoto K 2022 *Metrologia* **59** 035004

[16] Weyers S, Lipphardt B and Schnatz H 2009 *Phys. Rev. A* **79** 031803

[17] Weyers S, Gerginov V, Kazda M, Rahm J, Lipphardt B, Dobrev G and Gibble K 2018 *Metrologia* **55** 789

[18] Fang F, Chen W L, Liu K, Dai S Y, Liu N F, Han L and Zheng F S 2019 *Joint Conference of the European Frequency and Time Forum and IEEE International Frequency Control Symposium*, April 14-18, 2019, Orlando, Florida, USA (in Chinese)

[19] Liu D D, Ruan J, Fan S C, Zhang H, Guan Y, Wang X L, Shi J R, Yang F, Bai Y and Zhang S G 2020 *IEEE International Frequency Control Symposium and IEEE Symposium on Applications of Ferroelectrics*, July 19-23, 2020, Keystone, Colorado, USA (in Chinese)

[20] Abgrall M, 2003 Evaluation des performances de la fontaine atomique PHARAO, Participation à l'étude de l'horloge spatiale PHARAO (PhD Dissertation) (Univerisité Pierre et Marie Curie - Paris VI)

[21] Xue W X, Zhao W Y, Quan H L, Zhao C C, Xing Y, Jiang H F and Zhang S G 2020 *Chin. Phys. B* **29** 064209 (in Chinese)

[22] Bai Y 2025 *Research of Rubidium Atomic Fountain Clock on All-fiber Laser system* (PhD Dissertation) (Beijing: University of Chinese Academy of Sciences) (in Chinese)

[23] Zhang H 2023 *Development of time-keeping ^{87}Rb fountain clock* (PhD Dissertation) (Beijing: University of Chinese Academy of Sciences) (in Chinese)